Nanoscale

ROYAL SOCIETY OF CHEMISTRY

PAPER

View Article Online
View Journal | View Issue

Cite this: *Nanoscale*, 2023, **15**, 4591

Synchrotron radiation circular dichroism spectroscopy reveals that gold and silver nanoparticles modify the secondary structure of a lung surfactant protein B analogue†

Alison Buckley, [a] James Warren,[a] Rohanah Hussain [b] and Rachel Smith *[a]

Inhaled nanoparticles (NPs) depositing in the alveolar region of the lung interact initially with a surfactant layer and *in vitro* studies have demonstrated that NPs can adversely affect the biophysical function of model pulmonary surfactants (PS), of which surfactant protein B (SP-B) is a key component. Other studies have demonstrated the potential for NPs to modify the structure and function of proteins. It was therefore hypothesised that NPs may affect the biophysical function of PS by modifying the structure of SP-B. Synchrotron radiation circular dichroism (SRCD) spectroscopy was used to explore the effect of various concentrations of gold nanoparticles (AuNPs) (5, 10, 20 nm), silver nanoparticles (AgNPs) (10 nm) and silver citrate on the secondary structure of surfactant protein B analogue, SP-B_{1-25}, in a TFE/PB dispersion. For Au and Ag NPs the SRCD spectra indicated a concentration dependent reduction in the α-helical structure of SP-B_{1-25} (5 nm AuNP ≈ 10 nm AgNP >> 10 nm AuNP > 20 nm AuNP). For AuNPs the effect was greater for the 5 nm size, which was not fully explained by consideration of surface area. The impact of the 10 nm AgNPs was greater than that of the 10 nm AuNPs and the effect of AgNPs was greater than that of silver citrate at equivalent Ag mass concentrations. For 10 nm AuNPs, SRCD spectra for dispersions in, the more physiologically relevant, DPPC showed a similar concentration dependent pattern. The results demonstrate the potential for inhaled NPs to modify SP-B_{1-25} structure and thus potentially adversely impact the physiological function of the lung, however, further studies are necessary to confirm this.

Received 1st November 2022,
Accepted 6th January 2023

DOI: 10.1039/d2nr06107d

rsc.li/nanoscale

1. Introduction

Nanomaterials are an increasing part of modern life with a growing range of types and applications in consumer products.[1,2] However, concerns remain over their potential effects on human and environmental health. A particular issue is the effect of inhaled nanomaterials, as the human lung is sensitive to damage. Upon inhalation, nano-sized particles can reach the alveolar (gas exchange) region in the lung. As this is lined with an aqueous subphase fluid with an overlying surfactant layer,[3] initial particle interactions following alveolar deposition will be with this pulmonary surfactant. Pulmonary surfactant's primary physiological function is to stabilise alveoli and prevent alveolar collapse during breathing by reducing surface tension to near zero values at the end of exhalation and minimising the work of breathing.[4] It is therefore conceivable that direct interactions between inhaled nanoparticles (NPs) and pulmonary surfactant could affect the physiological function of the lung.[5]

Pulmonary surfactant comprises a mixture of phospholipids (~80%), neutral lipids (~10%) and proteins (~10%).[6] The most abundant component (~40%) is the phospholipid 1,2-dipalmitoyl-*sn-glycero*-3-phosphocholine (dipalmitolphosphatidylcholine, DPPC), which is a zwitterionic surfactant. To date four surfactant proteins (SPs) have been identified: SP-A, SP-B, SP-C and SP-D. Their functions are interrelated but primarily SP-A (~5–6%) and SP-D (~0.5%) play an important role in host immune defence (opsonins) and SP-B and SP-C in the biophysical functions of surfactant. SP-B and SP-C are small hydrophobic polypeptides each comprising around 1.0–1.5% of surfactant.[7] Optimised surfactant behaviour requires: (a) the effective transfer of the surfactant from the alveolar type II cells, where it is produced, through the aqueous phase to the interface, followed by interfacial adsorption of the active molecules to form the surface film; (b) surface tension reduction to

[a]*Toxicology Department, UK Health Security Agency, Harwell Science and Innovation Campus, Didcot, Oxfordshire, OX11 0RQ, UK. E-mail: Rachel.smith@ukhsa.gov.uk*
[b]*Diamond Light Source Ltd, Harwell Science and Innovation Campus, Didcot, Oxfordshire, OX11 0DE, UK*

† Electronic supplementary information (ESI) available. See DOI: https://doi.org/10.1039/d2nr06107d

values close to 0 mN m^{-1} during the compression of the respiratory surface at expiration; and, (c) efficient re-spreading of the surface film during expansion at inspiration. The phospholipids play a key role (*e.g.* DPPC can achieve surface tension values close to 0 mN m^{-1} on compression) but *in vitro* studies have indicated that the presence of the surfactant proteins is required to optimise the surfactant layer function, with proteins involved in promoting adsorption, stabilisation and re-spreading whilst lipids are essentially responsible for the significant surface tension reduction during compression.[8] In particular, SP-B, the only surfactant protein essential for life, is postulated to play key roles in interfacial adsorption and in the modification of lipid layer arrangements required for the conversion from mono- to multi- layers during respiration ("reservoir" formation).[7,9]

Langmuir–Wilhelmy Balance systems, pulsating bubble surfactometers, captive bubble tensiometers and constrained drop surfactometry, are frequently used to investigate surfactant function. Such methods monitor surface pressure during changes in surfactant monolayer area designed to mimic surface area changes in the lung during respiration and have been used widely to explore the impact of inhaled particles, including NPs, on lung surfactant model layers.[10] For example, the results of studies using DPPC as a model surfactant have varied with some indicating no or minimal effects of NPs on surface tension behaviour,[11] whilst others provide clear indications of negative changes to surface pressure-area isotherms.[12–16] Similar experiments have also been undertaken using more complete models of pulmonary surfactant for a limited range of nanomaterials and found a deterioration in surface tension behaviour.[17–20] For example, using the oscillating bubble technique, the effect of bare and coated polymeric NPs on the surface tension behaviour of a phospholipid mixture with and without the addition of different concentrations of SP-B and SP-C, alone and in combination, was investigated.[21] The study found that SP-C supplemented phospholipid mixtures were more susceptible to biophysical inactivation by bare NP than phospholipid mixtures supplemented with SP-B and that effects were reduced for coated particles. They hypothesised that overall surfactant function was hindered due to a significant depletion of the SP content upon contact with the bare NPs and undertook incubation studies of the NPs with the surfactant which indicated a loss of SPs from the surfactant consistent with the biophysical effects seen.

The results of these *in vitro* studies indicate that NPs have the potential to inhibit the function of surfactant films and that in more physiological relevant surfactant models these effects may be mediated by interactions of NPs with SPs.[11,18,21,22] Typical hypotheses in these cases relate to the impact of sequestration of surfactant, and in particular the protein components. These hypotheses either propose that SPs are present within the surfactant layer but bound to the NPs so that they are not able to perform their function, or that SPs bind to NPs which then leave the surfactant layer and are therefore removed from the system. Which of these mechanisms applies is considered dependent in a complex manner upon the physiochemical characteristics of the particles, including any coatings, in particular charge and hydrophobicity. For example, molecular dynamics modelling has indicated that model anionic hydrophilic NPs adsorb and pull SP-B_{1-25} out of a static surfactant monolayer.[23] These 'sequestration' hypotheses are supported by other studies which indicate that proteins and lipids can bind to NPs ("corona" formation), and recent *in vitro* studies have confirmed that particles interacting with human lung lining fluid acquire a biomolecular corona containing SP-B.[24,25]

An alternative to 'sequestration' hypotheses for the effect of NPs on the function of surfactant films containing SPs is the hypothesis that NPs modify the secondary structure of SPs,[26] which impacts on their behaviour (*e.g.* inactivates) within pulmonary surfactant and consequently affects surfactant film function. A number of studies, recently reviewed by Park (2020),[27] have found that NPs can modify the structure of proteins, with many studies indicating the following typical conformational changes: α-helical component decreases and/or β-sheet formation increases – with effects influenced by a range of factors including the nanomaterial type (including coating, functionalization *etc*.), size, shape, charge and concentration.[27] However, to date such studies have focussed on a limited range of proteins, in particular, bovine and human serum albumin, lysozyme and fibrinogen. The authors are not aware of any study on the effects of NPs on SP structure.

To address this gap, studies were undertaken of the effect of two types of NPs, gold (AuNP) and silver (AgNP), of a range of particle sizes and concentrations, on the secondary structure of a commonly used SP-B analogue, SP-B_{1-25}.[28] These NPs were chosen as they have been widely used in other studies. The majority of studies undertaken to explore the effects of NPs on the secondary structure of proteins have used circular dichroism (CD) spectroscopy,[27,29] however, to measure protein concentrations in the micromolar and submicromolar range, the use of longer pathlength cuvette cells (5 to 10 cm) with small apertures required the use of a highly incident collimated microbeam that can be provided only at the Diamond Light Source B23 beamline for synchrotron radiation circular dichroism (SRCD). These measurements are not possible with bespoke bench-top CD spectropolarimeters. This approach was used successfully by Laera *et al.* (2011)[30] to measure structural changes to a number of proteins exposed to NPs. Our study primarily used dispersions in Triflouroethanol (TFE), a commonly used solvent in CD studies, but DPPC was also used in some cases to represent a more physiologically realistic model.

2. Methods

2.1 Materials and sample preparation

The synthetic commonly used human SP-B analogue, SP-B_{1-25}, a 25-residue N-terminal segment of SP-B with amino acid sequence FPIPL PYCWL CRALI KRIQA MIPKG, was obtained from Invitrogen Life Technologies (UK) (see Fig. S1† for

peptide structure). Uncoated (*i.e.* no surface coating or functionalization) AuNPs of nominal diameters 5 nm, 10 nm and 20 nm in 0.1 mM phosphate buffered saline and uncoated AgNPs of nominal diameter 10 nm in 2 mM sodium citrate and were purchased from Cytodiagnostics (Burlington ON L7L 4X8, Canada).

Dispersions of Au and Ag NPs (a range of concentrations) and SP-B_{1-25}, separately and in combination, were produced in Triflouroethanol (TFE) with 4 mM phosphate buffer (PB). To explore the effect of silver ions compared with the silver nanoparticles, silver citrate ($Ag_3C_6H_5O_7^{3-}$) was used (Sigma-Aldrich, USA) in place of the AgNPs in some samples. Silver citrate concentrations were chosen so that the silver concentration matched the range of AgNP concentrations used. While TFE has the advantage of ease of use and readily promotes the helical structure in SP-B_{1-25}, it is not a physiologically relevant lung surfactant model. A preliminary investigation using DPPC (Sigma-Aldrich, USA), the main constituent of lung lining fluid, instead of TFE was therefore carried out with 10 nm AuNPs.

Preliminary optimisation experiments were undertaken, including, equipment calibration, sample cell choice and determination of optimum peptide/NP concentrations. For SP-B_{1-25} in TFE/PB, the best signal was achieved using a 5 cm path-length cell and a SP-B_{1-25} concentration of 4 μg ml^{-1} in TFE/4 mM phosphate buffer, 1 : 4 v : v. For DPPC, the ideal lipid: SP-B_{1-25} ratio would be close to that in the lung (~100 : 1, ref. 7). Using an SP-B_{1-25} concentration of 4 μg ml^{-1} though, the highest ratio achievable before absorbance became too great, was found to be 50 : 1. All DPPC samples were therefore made using 4 μg ml^{-1} SP-B_{1-25} in DPPC/4 mM PB, SP-B_{1-25}: DPPC, 50 : 1 v : v. The maximum NP concentration which could be used varied for the different materials/sizes investigated, but in general, concentrations greater than 10 μg ml^{-1} caused too much absorption at lower wavelengths. NP concentrations were chosen so that comparison of equivalent mass concentrations, surface area concentrations and ratios of free to bound SP-B_{1-25} could be made across the different particle sizes and materials. Table 1 details all the concentrations used, alongside calculations of number concentration, surface area concentration and estimates of the ratio of free to bound SP-B_{1-25}.

Ideally, the NP-peptide systems investigated would be such that there are no "free" peptides, *i.e.* peptide not interacting with the NP surface which could act to "dilute" any effects seen on the secondary structure of the "bound" peptides. Unfortunately, the minimum peptide concentration required to give sufficient CD signal, and issues with high absorbance of the SP-B, TFE and NPs at low wavelengths meant that this was not always possible here. Using a simple geometric model, assuming that the SP-B_{1-25} molecules are primarily α-helices of 12 Å diameter[31,32] which pack "end on" over the surface area of the nanoparticle sphere, the maximum theoretical number of SP-B_{1-25} molecules that can be packed around each NP are estimated to be 60, 240 and 961 for 5 nm, 10 nm and 20 nm diameter spherical NPs respectively. In reality many factors,

Table 1 Sample concentrations, estimated ratios of free to bound SP-B_{1-25} and secondary structure analysis

	Nanoparticle concentration			Ratio free/bound (SP-B_{1-25})	Protein conformation			
Sample	Mass (μg ml^{-1})	Particle no. (# ml^{-1})	Surface area (nm^2 ml^{-1})		α-Helix	β-Strand	Unordered	Turns
SP-B only (I)	0	0	0	na	24%	25%	29%	22%
SP-B only (II)	0	0	0	na	25%	25%	28%	22%
SP-B only (with sodium citrate)	0	0	0	na	28%	23%	25%	23%
5 nm AuNP	0.625	4.93×10^{11}	3.87×10^{13}	27	21%	30%	27%	22%
	1.25	9.85×10^{11}	7.73×10^{13}	13	14%	36%	27%	23%
	2.5	1.97×10^{12}	1.55×10^{14}	6	11%	37%	27%	25%
	5	3.94×1912	3.09×10^{14}	2	12%	38%	26%	23%
10 nm AuNP	1.25	1.23×10^{11}	3.87×10^{13}	27	24%	26%	29%	21%
	2.5	2.46×10^{11}	7.73×10^{13}	13	26%	24%	27%	23%
	5	4.93×10^{11}	1.55×10^{14}	6	18%	30%	29%	23%
	10	9.85×10^{11}	3.09×10^{14}	2	13%	35%	28%	24%
20 nm AuNP	1.25	1.54×10^{10}	1.94×10^{13}	55	28%	23%	26%	23%
	2.5	3.08×10^{10}	3.88×10^{13}	27	26%	23%	29%	21%
	5	6.16×10^{10}	7.76×10^{13}	13	25%	26%	26%	23%
	10	1.23×10^{11}	1.33×10^{14}	6	18%	32%	30%	19%
10 nm AgNP	0.3125	5.63×10^{10}	1.77×10^{13}	60	26%	24%	28%	22%
	0.625	1.13×10^{11}	3.53×10^{13}	29	19%	34%	24%	23%
	1.25	2.25×10^{11}	7.07×10^{13}	14	20%	21%	20%	24%
	2.5	4.50×10^{11}	1.41×10^{14}	7	12%	35%	29%	24%
Ag citrate[a]	1.05	na	na	na	23%	27%	28%	22%
	2.1	na	na	na	22%	29%	27%	21%
	4.21	na	na	na	23%	28%	25%	23%
	7.5	na	na	na	21%	29%	28%	22%

[a] Equivalent Ag+ concentrations of 0.625 μg ml^{-1}, 1.25 μg ml^{-1}, 2.5 μg ml^{-1} and 4.451 μg ml^{-1} respectively.

such as NP surface charge, size and surface curvature, pH and the presence of other ions can affect packing density and corona formation on metallic NPs[33] so these ratios are only intended to give an approximate indication of the level of binding of SP-B_{1-25} for comparative purposes.

As part of the preparatory work, sample mixing methods to ensure full dissolution of the SP-B_{1-25}, minimise NP agglomeration and to provide stable suspensions were devised. In summary, for TFE samples, NP stock solutions as provided by the manufacturer (20 μg ml^{-1} for 10 nm AgNPs, 69 μg ml^{-1}, 61 μg ml^{-1} and 53 μg ml^{-1} for 5 nm, 10 nm and 20 nm AuNPs respectively) were first diluted in milliQ water to the desired NP concentration and spiked with 0.2 ml of 0.1M PB to give the desired pH. 100% TFE or pre-prepared 20 μg ml^{-1} SP-B_{1-25} in TFE stock solution was then added to the NP suspension for buffer control and peptide samples respectively. Samples were then gently mixed with a pipette and rested for 1 hour before use. AuNP samples were found to be stable and resting time not to affect the CD results, but due to the potential for AgNPs to dissolve, resting times were kept consistent. For ionic silver samples, 10 μg ml^{-1} silver citrate in milliQ was added instead of the NP stock. For DPPC samples, DPPC (1 mg ml^{-1} in $CHCl_3$) and SP-B_{1-25} (0.1 mg ml^{-1} in MeOH) stocks were pre-prepared (DPPC only for buffers), mixed to give a peptide/lipid ratio of 50 : 1 and dried down in a fumehood. Approximately 1 hour before use, the powder was resuspended in milliQ and spiked with PB to give the desired pH (7.0) then vortex shaken and warmed at 47 °C in a water bath for 30 minutes. Samples were vortexed again and allowed to cool for at least 10 minutes before the NP stock was added and hand-shaken to give the desired NP concentration. Samples were then rested for 15 minutes before use.

2.2 Sample characterisation

Primary particles and particle agglomerates were visualised with high resolution transmission electron microscopy (TEM) (JEOL 3000 F, JEOL Inc., Tokyo, Japan) for all Au and Ag NPs at one concentration, both with and without SP-B_{1-25}. TEM samples were made by placing a few drops (10 μL) of NP dispersions, with time allowed for drying between drops, onto 400 mesh copper TEM grids with holey carbon films placed on filter paper and allowed to dry for 12 hours. NP primary particle diameters and agglomerate sizes were determined from the TEM images using image analysis software ImageJv1.52a[34] and used to estimate the NP number and surface area concentrations assuming spherical particles with bulk material density. For all TFE samples, the particle size distributions (hydrodynamic diameter), as determined by dynamic light scattering (Zetasizer Nano – ZS, Model ZEN3600, Malvern Instruments Ltd, UK) and pH (Jenway 3510 pH Meter, Cole-Parmer, UK) were measured at time of use. Zeta potential measurements of the Au and Ag NPs for a range of NP dispersions with TFE and SP-B_{1-25} were carried out in a separate investigation using the Zetasizer Nano – ZS (Model ZEN3600, Malvern Instruments Ltd, UK). These measurements were not possible for DPPC samples.

2.3 Synchrotron radiation circular dichroism measurements

Synchrotron radiation circular dichroism (SRCD) spectra were collected at the beamline B23 module end station B of Diamond Light Source (UK).[35–41] SRCD spectra were collected with a Suprasil cell of 5 cm path length (400 μL volume) (Hellma, Germany), with bandwidth of 1.2 nm, integration time of 1 s, 1 nm digital resolution, and 39 nm min^{-1} scan speed, and three or four repeated scans per spectrum for NP samples and buffers respectively. The sample cell was filled using a "drip-fill" method to reduce the chance of bubbles and left for 5 minutes before being placed in the instrument to allow gases to be released. Once installed, samples were rested for a further 3 minutes before running the scans. Spectral data was collected and processed using the CDApps software.[42] In short, repeated consecutive spectra have been averaged, corrected by subtraction of CD spectrum of the relevant buffer as baseline and smoothed by applying a 7 point Savitzky–Golay smoothing function. Analysis of the secondary structure of the SP-B_{1-25} was undertaken using the basis set SMP56, SP43 + 13 Membrane and two fitting algorithms, CONTINLL and CDSSTR.[43–45]

3. Results and discussion

3.1 Particle characterisation

Representative TEM images from selected dispersions are shown in Fig. 1 and 2 (additional images in Fig. S2†). The primary particle and surface area equivalent agglomerate diameters determined from the TEM images are summarised in Table 2. Images show that all NPs investigated are near spherical and show some evidence of crystalline structure but with a greater range of shapes and sizes observed for the AgNPs compared to the AuNPs (Fig. S2† and Table 2). Measured primary particle diameters are in good agreement with the manufacturer's data and remain unchanged by the addition of SP-B_{1-25}. Preparation of TFE suspensions caused agglomeration of both the Au and Ag NP primary particles, and the further addition of SP-B_{1-25} produced significantly larger agglomerates (2- to 8- fold) indicating that the protein is interacting with the NPs. This is as expected based on the respective positive and negative charges of the SP-B_{1-25} molecules and Au and Ag NPs.

The images (Fig. 1) suggest that "looser agglomerates", with more space observed between particles, were formed with SP-B_{1-25} for the 5 nm Au and 10 nm Ag NPs than other particles. Although TEM images were only taken for a limited range of concentrations it is assumed that, while the degree of agglomeration could vary with concentration, the overall conclusions regarding agglomeration by SP-B_{1-25} are relevant for all concentrations.

Dynamic light scattering measurements of hydrodynamic diameter confirmed the formation of NP agglomerates both with and without SP-B_{1-25}, with significantly greater agglomeration with SP-B_{1-25} compared to without (Table S1,† Fig. S3†). Unfortunately, there was significant variability in the

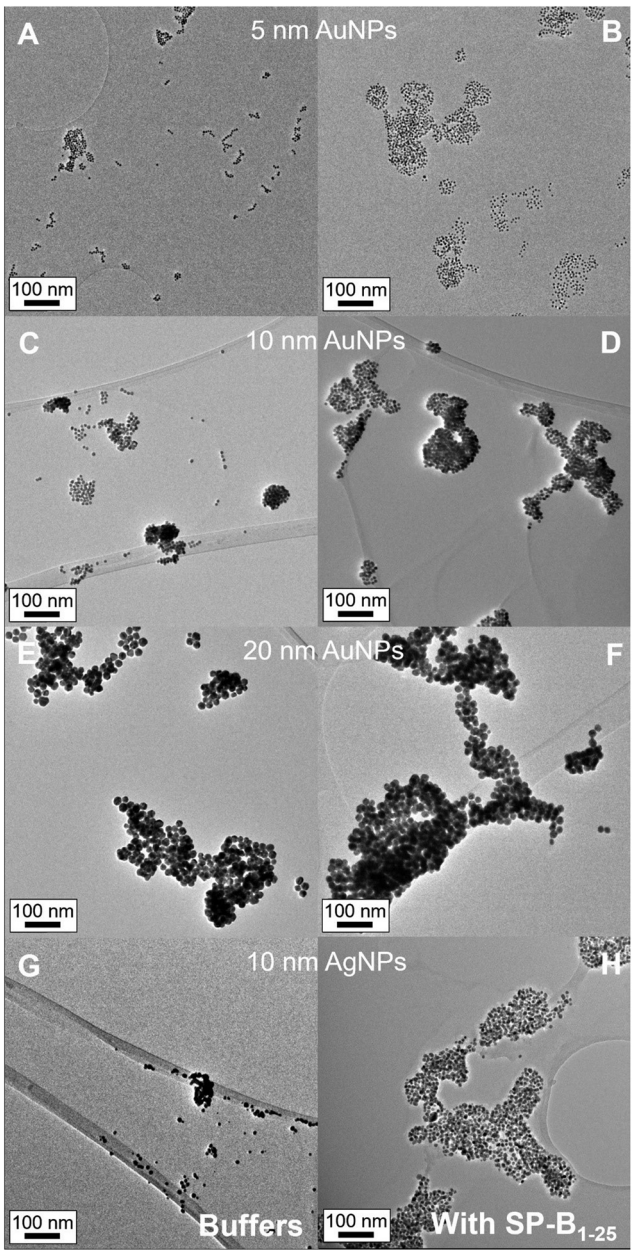

Fig. 1 Representative TEM images of 5 nm AuNPs (A) without and (B) with 4 μg ml^{-1} SP-B$_{1-25}$; 10 nm AuNPs (C) without and (D) with 4 μg ml^{-1} SP-B$_{1-25}$; 20 nm AuNPs (E) without and (F) with 4 μg ml^{-1} SP-B$_{1-25}$; 10 nm AgNPs (G) without and (H) with 4 μg ml^{-1} SP-B$_{1-25}$. AuNP and AgNP dispersions with concentrations 5 μg ml^{-1} and 2.5 μg ml^{-1} respectively in TFE/4 nM PB, 1 : 4 v : v. All images were taken at magnification 20000X with scale bars of 100 nm.

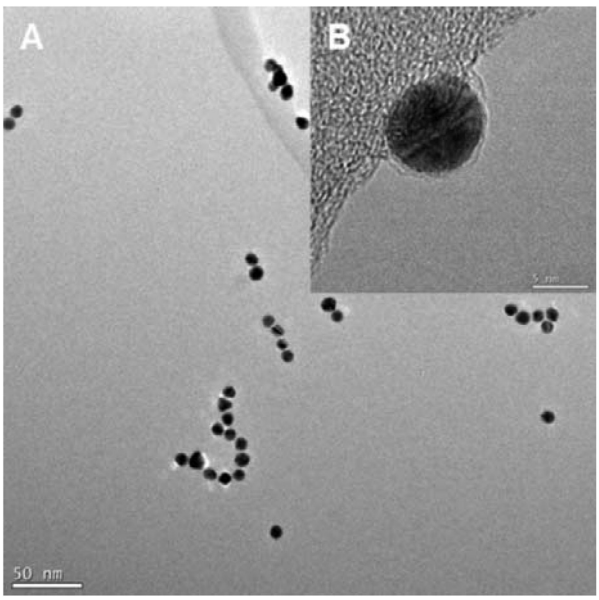

Fig. 2 Representative TEM images of 10 μg ml^{-1} 10 nm AuNPs with 4 μg ml^{-1} SP-B$_{1-25}$ and DPPC in 4 mM PB (DPPC/SP-B, 50 : 1 mol : mol), (A) taken at magnification 40 000× showing small agglomerates of the 10 nm AuNPs and (B) taken at magnification 500 000× showing crystalline structure of 10 nm AuNP and approximately 1 nm thick DPPC coating around the NP.

results and the absolute sizes measured are inconsistent with the TEM sizing, suggesting these results should be interpreted with caution. These results perhaps reflect the difficulties DLS is known to have in resolving the size distribution of complex mixtures.

The stability of the dispersions used was explored by undertaking separate measurements of the zeta potential of a limited number of additional dispersions similar to those used for the SRCD measurements and produced using the same protocols. Zeta potential measurements of all sizes of Au and Ag NPs in TFE/PB were negative, with values ranging between – 9 mV, for 10 nm Ag NPs, and –18 to −15 mV for Au NPs (Table S2†). Typically, zeta potentials >25 mV and <−25 mV represent stability, so these dispersions could be considered to display incipient instability. This is consistent with the development of agglomerates seen in the TEM images. The addition of SP-B$_{1-25}$ shifted the zeta potential towards positive values, indicating an association between the protein and the NPs, but at magnitudes that indicated a reduction in stability, consistent with an increase in agglomerate size, as seen. However, the range of NP concentrations considered did not fully overlap with that used for the SRCD measurements. It is recommended that for future studies zeta potential measurements are made of each experimental dispersion immediately prior to use.

In contrast to the TFE suspensions, agglomerates remained small after addition of SP-B$_{1-25}$ to the DPPC suspension (Table 2 and Fig. 2). TEM images of the 10 nm AuNPs in DPPC/SP-B$_{1-25}$ also show evidence of a coating, presumably of DPPC and SP-B, approximately 1 nm thick (Fig. 2), not observed for the NPs in TFE/SP-B. This coating may stabilise the NP suspension and thus limit agglomeration. Dynamic Light Scattering measurements were not made of any DPPC samples.

The pH of the TFE/PB study samples ranged from 5.2–6.4. Whilst this is slightly more acidic than typical quoted values for the alveolar subphase fluid of 6.9,[6] it has been hypoth-

Table 2 Primary particle and agglomerate sizes from TEM images (unless otherwise stated, $N = 75$)

	Primary particle diameter (Average ± SD) (nm)			Agglomerate surface area equivalent diameter (Average ± SD) (nm)	
Nanoparticle[a]	Manufacturer's data	Without SP-B_{1-25}	With SP-B_{1-15}	Without SP-B_{1-25}	With SP-B_{1-15}
5 nm Au	5 ± 15	5.4 ± 0.5	5.4 ± 0.6	19.3 ± 13.7 ($N = 47$)	138.9 ± 96.8 ($N = 40$)
10 nm Au	10 ± 2	9.4 ± 0.9	9.4 ± 0.9	34.7 ± 31.1 ($N = 83$)	84.8 ± 54.6 ($N = 59$)
20 nm Au	20 ± 15	19.9 ± 2.4	19.9 ± 3.0	72.4 ± 48.3 ($N = 55$)	131.5 ± 135.4 ($N = 22$)
10 nm Ag	10 ± 3	9.0 ± 3.0	8.9 ± 2.8	20.0 ± 18.1 ($N = 136$)	126.0 ± 139.5 ($N = 29$)
10 nm Au (in DPPC)	10 ± 2	—	9.6 ± 0.9 ($N = 65$)	—	17.0 ± 11.5 ($N = 27$)

[a] In TFE unless otherwise stated.

esised that there could be localised variability in pH due to the presence of alveolar macrophages.[6] However, studies of the effect of pH on the surface tension behaviour of a range of surfactants have indicated that natural lung surfactants are not significantly affected over a pH range from 3–7.5 and that generally a range of 5.0–7.4 is considered optimal for surfactant studies.[46]

3.2 CD spectra and secondary structure analysis

Fig. 3(A–E) shows the SRCD spectra for SP-B_{1-25} and all the NP-SP-B_{1-25} dispersions in TFE investigated at a range of concentrations and Fig. 3(F) shows the spectra for SP-B_{1-25} with a range of silver citrate concentrations chosen to give equivalent silver concentrations as used for the NP investigation. The spectra of SP-B_{1-25} only, dispersed in TFE, show double minima at approximately 208 nm and 222 nm, features characteristic of α-helical secondary structure and consistent with spectra of SP-B[47] and SP-B_{1-25}[48] in organic solvents. In general, the addition of NPs causes a clear change in the CD spectra indicative of changes in secondary structure as a consequence of nanoparticle-peptide interactions, the extent of which increases with NP concentration. Whilst all the NPs investigated produced the same general trend in terms of spectral shape change with increasing NP concentration, the absolute changes per unit increase in mass concentration vary between NPs. For example, an 8-fold greater NP concentration (10 μg ml^{-1}) is required for the 10 nm AuNPs to produce a similar spectral shape to that of the 10 nm AgNPs at 1.25 μg ml^{-1}. This effect is highlighted further in Fig. 4(A) which shows the variation in CD spectrum value at 208 nm (corresponding to the first trough in the SP-B_{1-25} CD spectra) with NP mass concentration for the 4 NPs investigated. Two clear groupings can be seen, with the effects of the NPs in the order: 5 nm AuNPs ≈ 10 nm AgNPs >> 10 nm AuNPs > 20 nm AuNPs.

To investigate the changes in the CD spectra further, secondary structure analysis of the SP-B_{1-25} spectra using the software CDApps[42] was carried out. Two fitting algorithms, CONTINLL and CDSSTR, were used with the basis set SMP56 consisting of 43 soluble proteins and 13 membrane proteins.[43–45] All fits for both algorithms were within the acceptable standard deviation ranges (<0.07 for CONTINLL and <0.25 for CDSSTR), and the values obtained using both were very consistent. Table 1 gives the α-helix, β-strand, unordered and turn components obtained for each NP-peptide complex as the average of the two algorithms. Fig. 4 shows the α-helix component as a function of NP mass concentration and NP primary particle surface area concentration for all the Au and Ag NP samples analysed, and as a function of silver mass concentration for the silver citrate samples, compared to the results for 10 nm AgNPs.

For all NPs investigated, there is a clear trend of decreasing percentage of α-helix with increasing NP mass concentration (Fig. 4B); the extent of which varies between the particle sizes and materials investigated. The AuNPs, for example, show an increasing effect with decreasing particle size. Assuming that the change in secondary structure of the SP-B_{1-25} is due to a physical interaction with the NP surface, then this is to be expected, as the same mass concentration of different sized particles will have a different surface area available for binding, and indeed, the results for 20 nm and 10 nm AuNPs expressed in terms of primary particle surface area (Fig. 4C) are very similar. However, the results for 5 nm AuNPs and 10 nm AgNPs remain more significant even after surface area has been taken into consideration. Fig. S4† shows that for all the nanoparticles investigated, a decrease in the α-helical component of SP-B_{1-25}'s secondary structure corresponded to an increase in amount of β-strand but had no effect on the unordered or turn component.

Fig. 5 shows the results for the SRCD measurements made of SP-B_{1-25} in DPPC (50 : 1 mol : mol) with and without 10 nm AuNPs. While the magnitude of the CD signal was smaller, and noise greater for SP-B_{1-25} dispersed in DPPC, averaging 3 consecutive data sets clearly shows the same characteristic spectral shape as for SP-B_{1-25} in TFE and consistent with CD spectra for SP-B_{1-25} in a similar lipid mixture (DPPC : POPG, 4 : 1).[49] Similarly to the TFE dispersions, with the addition of 10 nm AuNPs, a clear reduction in the magnitude of the spectra minima is observed (see table in Fig. 5), the extent of which increases with NP concentration. The rate of change with increasing concentration is slightly greater for the 208 nm minima compared to the 222 nm minima for both TFE and DPPC, leading to a 'skew' in the CD spectra as the nanoparticle concentration increases, and a decrease in the

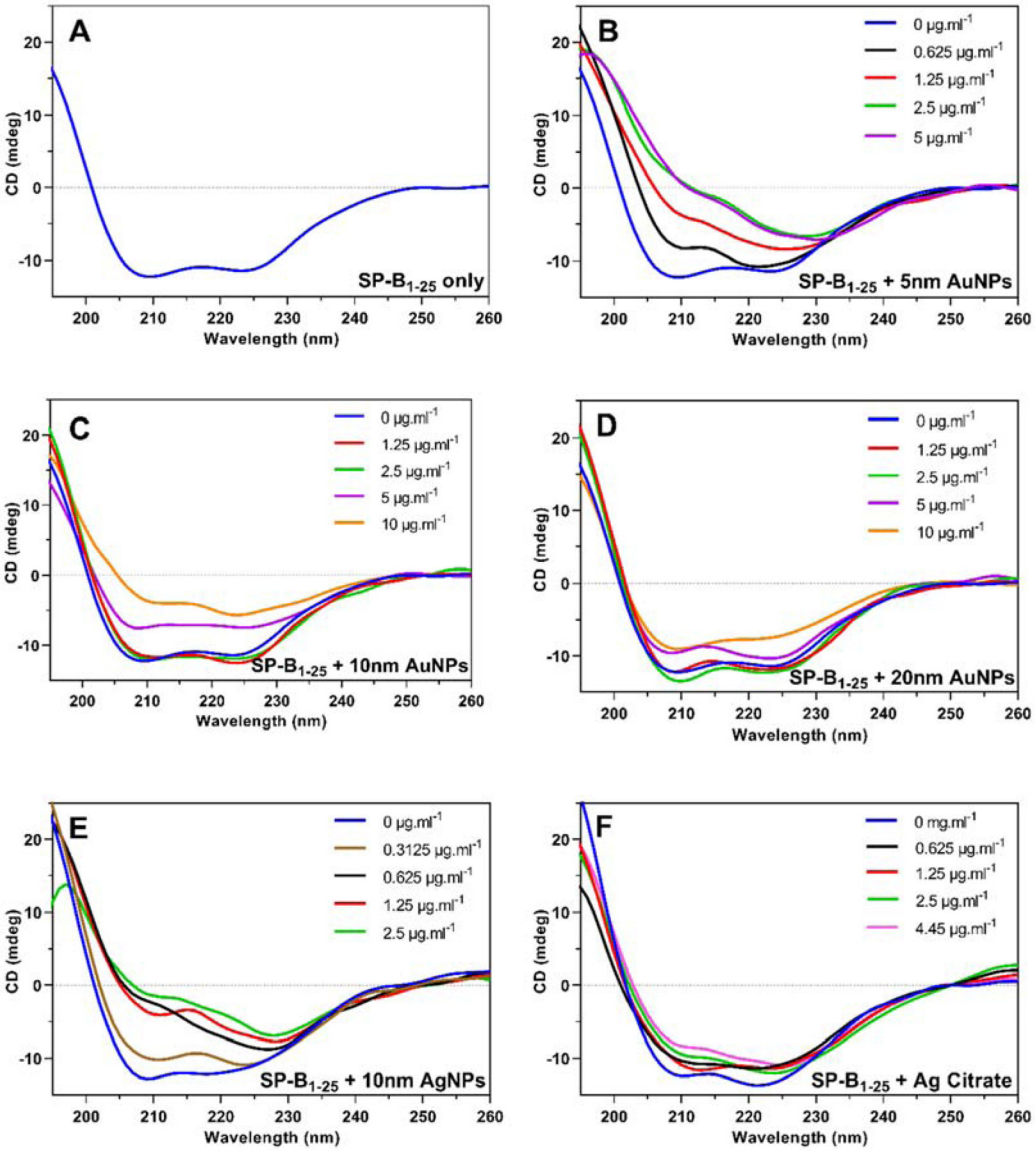

Fig. 3 SRCD spectra of peptide-NP complexes at varying NP concentrations (the colours used for a given concentration are consistent across all plots) and free peptide (blue line). (A) SP-B_{1-25} only; (B) SP-B_{1-25}-5 nm AuNPs; (C) SP-B_{1-25}-10 nm AuNPs; (D) SP-B_{1-25}-20 nm AuNPs; (E) SP-B_{1-25}-10 nm AgNPs; and (F) SP-B_{1-25} with varying concentrations of silver citrate (note concentrations given are Ag mass concentration for comparison to AgNP concentrations and not Ag citrate concentration), all in TFE/4 mM PB, 1 : 4 v : v with SP-B_{1-25} concentration 4 μg ml^{-1}.

ratio of ellipticities at 208 nm and 222 nm, a parameter sensitive to changes in the CD spectrums shape.[47]

As secondary structure analysis using CDApps was not possible for the DPPC samples, secondary structure was estimated using the BeStSel web application.[50,51] While results suggest a similar effect on the secondary structure of the SP-B_{1-25} in DPPC as for TFE with the addition of 10 nm AuNPs, firm conclusions cannot be drawn without further work. See ESI (Fig. S5†) for the results of the BeStSel analysis and further discussion.

Comparing the results for AgNPs and silver citrate for similar silver concentrations (Fig. 3 and 4) indicates that the ionic silver has a much less significant impact on the protein structure than the NPs, highlighting the effect of the particle surface on the protein conformation.

3.3 Summary of results and comparison to literature

Overall, the results show that in this simplified system, interaction with Au and Ag NPs causes conformational changes to SP-B_{1-25}, reducing the helical structure and increasing the β-strand, in both TFE and DPPC. These results are consistent with other studies indicating that NPs have the potential to reduce α-helical structure of proteins and increase β-sheet formation (see Park *et al.* 2020[27] for a recent summary of the available literature). However, this is the first study we are aware of to be conducted on surfactant proteins.

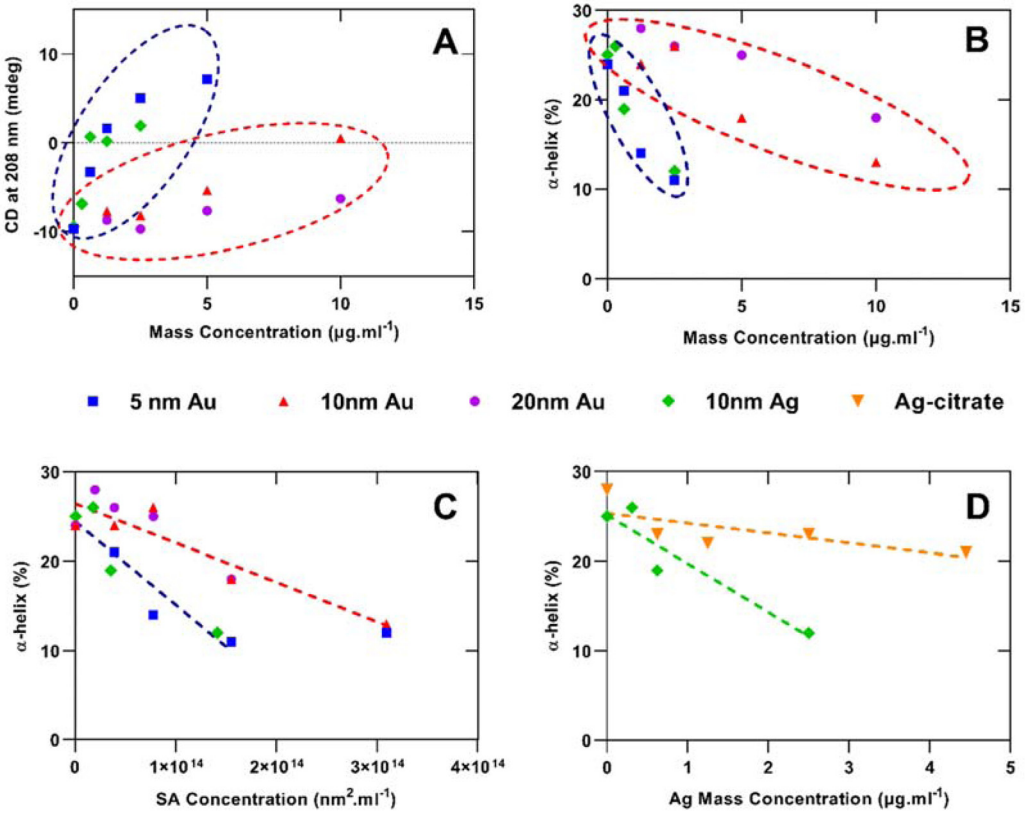

Fig. 4 Spectral Analysis: (A) CD at 208 nm with NP mass concentration for the NPs investigated; (B) and (C) give the α-helix component as a function of particle mass concentration and primary particle surface area concentration respectively for NP + SP-B_{1-25} + TFE/PB dispersions with Au and Ag NPs, and; (D) the α-helix component as a function of silver mass concentration for the silver citrate samples, compared to the results for 10 nm Ag nanoparticles. All in TFE/4 mM PB, 1 : 4 v : v with SP-B1$_{-25}$ concentration 4 μg ml^{-1}. Bounding circles and dashed lines are shown to highlight trends and groupings.

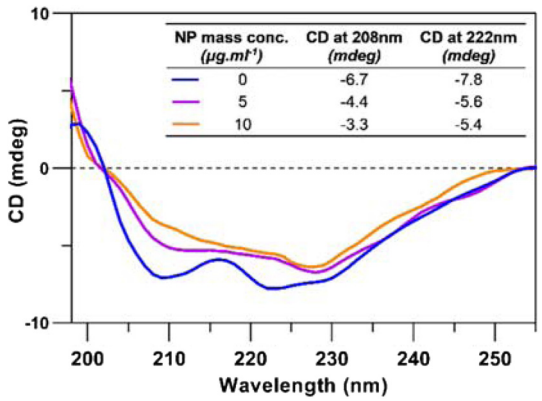

Fig. 5 SRCD spectra of free SP-B_{1-25} (blue line) and SP-B_{1-25} with 10 nm AuNPs (purple and orange lines), all in DPPC/4 mM PB, DPPC/SP-B_{1-25}, 50 : 1 mol : mol. The table insert shows the CD values at the two minima for each concentration presented.

For both NP types and all sizes investigated we observed an increase in conformational change of SP-B_{1-25} with greater β-strand content at the expense of α-helix with increased NP concentration expressed as either mass, particle number concentration (not shown) or primary particle surface area. This has been reported in other studies, for example, Capomaccio *et al.* observed a decrease in the α-helicity of HSA (human serum albumin) produced by exposure to 14 nm AuNPs that increased with concentration.[52] Such findings are consistent with a primary hypothesis of surface interactions leading to conformation changes. The similarity between these results for the 20 nm and 10 nm AuNPs expressed in terms of primary particle surface area (Fig. 4) supports the importance of this parameter.

The effects of 5 nm AuNPs, however, remain more significant than for the larger AuNPs even when primary particle surface area is taken into account. There are a number of potential explanations for this difference. The estimates of bound and free proteins were undertaken using the same simplistic assumptions for each particle size (including complete monolayer coverage). It is possible though that binding is proportionally greater for the smaller particles (the qualitatively looser agglomerates for the 5 nm AuNPs (Fig. 1) may suggest a greater binding potential, although this would clearly require further investigation). This would be consistent with the findings of Hill *et al.* 2009[53] on the loading of oligonucleotides on AuNPs (range 10 nm – 200 nm), which found that loading (per unit surface area) decreased approximately exponentially with

increasing radius until around 60 nm after which values remained broadly constant and comparable to values for planar surfaces. They hypothesised that this was due to increased deflection between strands and decreased steric interaction. Zhang *et al.*[54] also found that smaller AgNPs (16 nm) produced a greater reduction in α-helicity of HSA than larger (26 and 40 nm). Other studies have, however, indicated the opposite effect with larger particles resulting in proportionally greater protein binding[55,56] and/or causing more significant effects on protein secondary structure[57,58] than smaller.

It is clear that the degree of protein binding and conformational changes depend in a complex manner on the physiochemical characteristics of the NPs and the characteristics of the protein and biological environment (see previous reviews[27,33,59]). For example, Qu *et al.* found differences in binding and conformation changes of HSA with Quantum Dots with different ligands,[60] and modelling undertaken by Khan *et al.*[61] indicated that the orientation of proteins on NPs varied with particle size, with the orientation switching from one conformation to another at 12 nm for ubiquitin and 3–5 nm for insulin and haemoglobin. For human serum albumin, four different orientations were identified relating to the following particle sizes: 1–3, 4–10, 11–20 and >20 nm. Differences in orientation would be expected to impact on corona formation including the density of packing.

As well as the difference between 5 nm and larger AuNPs, the degree of conformational change induced by the 10 nm AgNPs was markedly greater than that for AuNPs of the same size and surface area concentration. Silver is intrinsically more soluble than gold so one possible hypothesis for the difference is that silver ions released from the AgNPs are affecting the protein structure. However, our results comparing AgNPs with silver ions of equivalent mass (Fig. 3 and 4) indicate minimal effects on the protein secondary structure of the silver ions. The difference between the results for 10 nm Au and 10 nm Ag NPs may be a result of differences in protein binding arising from the presence of citrate in the Ag but not the Au dispersion, and this could usefully be investigated further. Other studies have indicated that the type of nanoparticle can have a significant impact on protein binding, *e.g.* more plasma protein bound to silica than polystyrene NPs of the same size at low plasma protein concentrations.[62] Lai *et al.*,[63] examined the protein corona formed from human plasma on 20 nm Au and Ag NPs with different surface modifications and found differences in the characteristics of the corona (size, constituent proteins) related both to the core material and surface charge.

3.4 Experimental limitations

The SP-B_{1-25} only CD spectra observed in this study show double minima at approximately 208 nm and 222 nm, features characteristic of α-helical secondary structure and consistent with spectra of SP-B[47] and SP-B_{1-25}[48] in organic solvents and lipids. The derived α-helix content for SP-B_{1-25} in TFE (*ca.* 30%) was, however, lower than that seen in other studies using solvents (*e.g.* 37% in methanol measured using Fourier transform infrared spectroscopy[48]). It is unclear why this difference is seen and this requires further consideration, although this does not affect the overall findings of this study, which relate to the incremental effects of the NPs. This difference is more marked for the SP-B_{1-25} in DPPC spectra, however, this was a preliminary investigation with limited, lower quality data and clearly requires further optimisation.

TFE is clearly not physiologically relevant, and some experts advise against the use of organic solvents, including TFE, in CD spectroscopy due to the potential for effects of solvents on protein structure,[29] however, TFE is widely used in CD and a study considering the structure of porcine extracted SP-B in a range of TFE/water mixtures found that SP-B maintained a very stable conformation in mixtures containing up to 70% TFE.[47] The same research group also found that the conformation of SP-B in TFE (70%) and DPPC vesicles was very similar.[64] However, experiments with more realistic models reflecting the range of lipids and proteins present in lung surfactant are necessary to confirm the findings as relevant to complete surfactant as the interactions between NP and SP-B_{1-25} may be affected by the presence of other biomolecules.

TFE may also contribute to the NP agglomeration observed in suspensions both with and without SP-B_{1-25} (Fig. 1, Table 2 and Table S1, Fig. S3†). In contrast, only minimal agglomeration was observed for DPPC suspensions. NP agglomeration, prior to the addition of SP-B_{1-25}, leads to uncertainty in the surface area available for binding. Depending on the strength of the adhesive forces holding the NPs together, a smaller surface area could be available for binding with SP-B_{1-25}. While the absolute surface area available for binding may be uncertain, and therefore the degree of "dilution" of any conformational changes observed caused by any unbound SP-B_{1-25} in the suspension, it does not negate the fact that conformational changes were observed due to the interaction of Au and Ag NPs with SP-B_{1-25}. To limit this uncertainty though, in any future work, using DPPC to suspend the SP-B_{1-25} would not only be more realistic, but also limit agglomeration, however, this would require improvements in signal strength.

Comparison studies *in vitro* have indicated that SP-B_{1-25} functions similarly to complete SP-B (*e.g.* Lipp *et al.*[65]) and *in vivo* studies in deficient animal models have confirmed improvements in lung function using this analogue.[66,67] Although it is not as effective as the dimeric form and cannot replicate the full functions of native SP-B as effectively as some more complete analogues.[28,68] Additional studies would be needed to confirm the relevance of these findings to the complete protein, which may for example, exhibit different binding patterns.

To probe any conformational change in SP-B_{1-25} when adsorbed on the NP surface, ideally the NP-peptide system would be such that there are no "free" peptides. This requires a very low concentration of the mixture. Measurement of conformational changes of proteins by CD spectroscopy in submicromolar concentrations can only be achieved using a long pathlength cell. SRCD measurement at the Diamond Light

Source B23 beamline, with its highly collimated beam, allows the measurement of very low volume samples of micromolar and sub-micromolar concentrations (~300–600 μL) using a long pathlength, small aperture cell. A previous study using protein concentrations similar to those used here indicated that such measurements could not be undertaken using bench top CD instruments, due to the large highly divergent beam.[69] Unfortunately, in this study the minimum peptide concentration required to give sufficient signal, and issues with the high absorbance of the SP-B_{1-25}, TFE and NPs at low wavelengths meant that "free" peptide was probably present in all samples (estimates using simple geometric consideration, Table 1). Consideration should be given in future studies to improving the ratio of free to bound peptide, perhaps using experimental protocols to remove the unbound protein from the suspension and/or techniques to quantify the bound peptide, and potentially the use of NP and protein concentrations which are more environmentally and physiologically relevant.

3.5 What about our hypothesis?

As discussed in the Introduction, the results of *in vitro* studies indicate that NPs have the potential to inhibit the function of pulmonary surfactant model films and that in more physiological relevant surfactant models these effects may be mediated by interactions of NPs with SPs. Typical hypotheses in these cases relate to the impact of sequestration of surfactant, and in particular the protein components by NPs. These hypotheses either propose that SPs are present within the surfactant layer but bound to the NPs so that they are not able to perform their normal function, or that SPs bind to NPs which then leave the surfactant layer and therefore are removed from the system.

On the basis of previous studies demonstrating the ability of NPs to modify protein secondary structure (*e.g.* as reviewed by Park[27]), we posited an alternative hypothesis, *i.e.* NPs modify the secondary structure of SPs, which affects their behaviour (*e.g.* inactivates) within pulmonary surfactant and consequently adversely affects surfactant film function. In this study we have explored this hypothesis using two types of NPs and demonstrated that both Au and Ag NPs can modify the structure, and therefore have implications for the proper functioning of, an SP-B analogue, SP-B_{1-25}. Whilst consideration of the structure of the complete SP-B molecule suggests that this would also be similarly affected, this remains to be confirmed and may differ in degree. Additional studies using other NPs are also required to test whether these findings are broadly applicable or only valid for specific types of NPs. Whether changes to the secondary structure of SP-B impacts on model pulmonary surfactant film behaviour would also require investigation to fully test this hypothesis.

Further studies of surfactant film behaviour could then usefully be undertaken to investigate whether for specific NPs either 'sequestration' or 'modification' act alone or in combination to produce any effects seen. These should consider the NP biomolecular corona. It is known that these can be dynamic, undergoing exchange with the surrounding medium (*i.e.* it is possible that adsorbed and modified SP-B could be released and reincorporated in the surfactant layer). Results of a recent review suggest that the position regarding the reversibility, or otherwise, of adsorption of a specific protein on NPs is unclear, with findings varying with many factors including, particle type and size, the characteristics of the medium (*e.g.* number and type of proteins) and experimental factors, such as time and concentrations.[70] Such studies should reflect relevant physiological timescales by considering the metabolism of SP-B. The main components of surfactant are produced in alveolar type II cells. The lipids and SP-B and SP-C are secreted together in lamellar bodies into the hypophase, these 'unravel' to form tubular myelin and large lipid arrays which adsorb to the interface to form the surface film. After 'use' the surfactant is partly recycled by type II cells (*e.g.* 50% recycling DPPC in rabbits) with the remainder catabolised by macrophages or type II cells with biological half-times of phosphatidylcholine species ranging from 8 to 12 h in mice, rats and rabbits, with shorter biological turnover times because of recycling.[71] Similar recycling of SP-B has been demonstrated in animal models, although different half-times have been seen: 28 h in mice (DPPC ~11 h)[72] and 7 h (DPPC ~11 h) in mature rabbits.[73] These are broadly consistent with values for newborn infants, 21 h (8–35 h).[74]

It is accepted that the use of surfactant film model systems are very useful for identifying the potential impact of particulate matter, however, they cannot reflect all physiological aspects of the system.[10] To discover whether any modifications seen *in vitro* to surfactant model function by NPs translate to physiological effects (*i.e.* negative impact on breathing) would require the use of *in vivo* models. It is important that such studies use realistic NP exposure levels.

Further investigation may indicate that effects on surfactant protein structure could be one form of molecular initiating event (MIE) leading to decreased lung function (adverse outcome (AO)) and therefore potentially contribute to the future development and expansion of the Adverse Outcome Pathway (AOP) developed by Da Silva *et al.* (2021) – lung surfactant function inhibition (MIE) leading to decreased lung function (AO) (**https://www.aopwiki.org/aops/302** and **https://aopkb.oecd.org**).[75]

4. Conclusions

Surfactant protein B plays a key role in the biophysical function of lung surfactant and is essential to life. In this study, to our knowledge the first of its kind, we have investigated the impact of nanoparticles on the secondary structure of a synthetic SP-B analogue (corresponding to the N-terminal residues 1–25 of SP-B) using SRCD at the Diamond Light Source B23 beamline. Our studies have demonstrated that Au and Ag nanoparticles can cause conformational changes in the structure of a key component of SP-B, which could change its effect *in vivo*, potentially leading to alterations in lung surfactant

function and ultimately the physiological behaviour of the lung. However, as identified, further work is needed to confirm and extend these initial findings (*e.g.*, to other types of nanoparticles) and explore their potential impact, including detailed consideration of SP-B within the context of the nanoparticle biomolecular corona.

Conflicts of interest

There are no conflicts to declare.

Acknowledgements

We acknowledge the support of Diamond Light Source for time on Beamline B23 (Proposals: SM8475 and SM9567) and Professor Giuliano Siligardi for technical support and useful discussions and Professor Tim Gant, Dr Tim Marczylo and Dr Martin Leonard for practical assistance and advice.

References

1 S. F. Hansen, L. R. Heggelund, P. R. Besora, A. Mackevica, A. Boldrin and A. Baun, Nanoproducts – what is actually available to European consumers?, *Environ. Sci.: Nano*, 2016, **3**, 169–180.
2 M. E. Vance, T. Kuiken, E. P. Vejerano, S. P. McGinnis, M. F. Hochella Jr., D. Rejeski and M. S. Hull, Nanotechnology in the real world: Redeveloping the nanomaterial consumer products inventory, *Beilstein J. Nanotechnol.*, 2015, **6**, 1769–1780.
3 E. R. Weibel and J. Gil, Electron microscopic demonstration of an extracellular duplex lining layer of alveoli, *Respir. Physiol.*, 1968, **4**, 42–57.
4 L. Knudsen and M. Ochs, The micromechanics of lung alveoli: structure and function of surfactant and tissue components, *Histochem. Cell Biol.*, 2018, **150**, 661–676.
5 C. Schleh and J. M. Hohlfeld, Interaction of nanoparticles with the pulmonary surfactant system, *Inhalation Toxicol.*, 2009, **21**, 97–103.
6 A. W. Ng, A. Bidani and T. A. Heming, Innate host defense of the lung: effects of lung-lining fluid pH, *Lung*, 2004, **182**, 297–317.
7 J. C. Castillo-Sánchez, A. Cruz and J. Pérez-Gil, Structural hallmarks of lung surfactant: Lipid-protein interactions, membrane structure and future challenges, *Arch. Biochem. Biophys.*, 2021, **703**, 108850.
8 A. G. Serrano and J. Pérez-Gil, Protein-lipid interactions and surface activity in the pulmonary surfactant system, *Chem. Phys. Lipids*, 2006, **141**, 105–118.
9 E. J. Veldhuizen, J. J. Batenburg, L. M. van Golde and H. P. Haagsman, The role of surfactant proteins in DPPC enrichment of surface films, *Biophys. J.*, 2000, **79**, 3164–3171.
10 E. Guzmán, Fluid Films as Models for Understanding the Impact of Inhaled Particles in Lung Surfactant Layers, *Coatings*, 2022, **12**, 277.
11 S. Tatur and A. Badia, Influence of Hydrophobic Alkylated Gold Nanoparticles on the Phase Behavior of Monolayers of DPPC and Clinical Lung Surfactant, *Langmuir*, 2012, **28**, 628–639.
12 E. Guzmán, E. Santini, D. Zabiegaj, M. Ferrari, L. Liggieri and F. Ravera, Interaction of Carbon Black Particles and Dipalmitoylphosphatidylcholine at the Water/Air Interface: Thermodynamics and Rheology, *J. Phys. Chem. C*, 2015, **119**, 26937–26947.
13 R. K. Harishchandra, M. Saleem and H.-J. Galla, Nanoparticle interaction with model lung surfactant monolayers, *J. R. Soc., Interface*, 2010, **7**, S15–S26.
14 D. Kondej and T. R. Sosnowski, Effect of clay nanoparticles on model lung surfactant: a potential marker of hazard from nanoaerosol inhalation, *Environ. Sci. Pollut. Res.*, 2016, **23**, 4660–4669.
15 M. M. Diez, A. Buckley, T. D. Tetley and R. Smith, The method of depositing CeO_2 nanoparticles onto a DPPC monolayer affects surface tension behaviour, *NanoImpact*, 2019, **16**, 100186.
16 S. S. You, C. T. R. Heffern, Y. Dai, M. Meron, J. M. Henderson, W. Bu, W. Xie, K. Y. C. Lee and B. Lin, Liquid Surface X-ray Studies of Gold Nanoparticle–Phospholipid Films at the Air/Water Interface, *J. Phys. Chem. B*, 2016, **120**, 9132–9141.
17 Y. Chen, Y. Yang, B. Xu, S. Wang, B. Li, J. Ma, J. Gao, Y. Y. Zuo and S. Liu, Mesoporous carbon nanomaterials induced pulmonary surfactant inhibition, cytotoxicity, inflammation and lung fibrosis, *J. Environ. Sci.*, 2017, **62**, 100–114.
18 Q. Fan, Y. E. Wang, X. Zhao, J. S. C. Loo and Y. Y. Zuo, Adverse biophysical effects of hydroxyapatite nanoparticles on natural pulmonary surfactant, *ACS Nano*, 2011, **5**, 6410–6416.
19 E. Guzmán, E. Santini, M. Ferrari, L. Liggieri and F. Ravera, Evaluating the Impact of Hydrophobic Silicon Dioxide in the Interfacial Properties of Lung Surfactant Films, *Environ. Sci. Technol.*, 2022, **56**(11), 7308–7318.
20 Y. Yang, Y. Wu, Q. Ren, L. G. Zhang, S. Liu and Y. Y. Zuo, Biophysical Assessment of Pulmonary Surfactant Predicts the Lung Toxicity of Nanomaterials, *Small Methods*, 2018, **2**(4), 1700367.
21 M. Beck-Broichsitter, C. Ruppert, T. Schmehl, A. Günther and W. Seeger, Biophysical inhibition of pulmonary surfactant function by polymeric nanoparticles: Role of surfactant protein B and C, *Acta Biomater.*, 2014, **10**, 4678–4684.
22 M. Beck-Broichsitter and A. Bohr, Bioinspired polymer nanoparticles omit biophysical interactions with natural lung surfactant, *Nanotoxicology*, 2019, **13**, 964–976.
23 G. Hu, B. Jiao, X. Shi, R. P. Valle, Q. Fan and Y. Y. Zuo, Physicochemical properties of nanoparticles regulate translocation across pulmonary surfactant monolayer and for-

mation of lipoprotein corona, *ACS Nano*, 2013, **7**, 10525–10533.

24 A. Kumar, E. M. Bicer, A. B. Morgan, P. E. Pfeffer, M. Monopoli, K. A. Dawson, J. Eriksson, K. Edwards, S. Lynham, M. Arno, A. F. Behndig, A. Blomberg, G. Somers, D. Hassall, L. A. Dailey, B. Forbes and I. S. Mudway, Enrichment of immunoregulatory proteins in the biomolecular corona of nanoparticles within human respiratory tract lining fluid, *Nanomedicine*, 2016, **12**, 1033–1043.

25 H. Whitwell, R.-M. Mackay, C. Elgy, C. Morgan, M. Griffiths, H. Clark, P. Skipp and J. Madsen, Nanoparticles in the lung and their protein corona: the few proteins that count, *Nanotoxicology*, 2016, **10**, 1385–1394.

26 D. Q. Arick, Y. H. Choi, H. C. Kim and Y. Y. Won, Effects of nanoparticles on the mechanical functioning of the lung, *Adv. Colloid Interface Sci.*, 2015, **225**, 218–228.

27 S. J. Park, Protein-Nanoparticle Interaction: Corona Formation and Conformational Changes in Proteins on Nanoparticles, *Int. J. Nanomed.*, 2020, **15**, 5783–5802.

28 F. J. Walther, L. M. Gordon and A. J. Waring, Design of Surfactant Protein B Peptide Mimics Based on the Saposin Fold for Synthetic Lung Surfactants, *Biomed. Hub*, 2016, **1**, 1–21.

29 ISO, Nanotechnologies—Assessment of protein secondary structure during an interaction with nanomaterials using ultraviolet circular dichroism, 2021.

30 S. Laera, G. Ceccone, F. Rossi, D. Gilliland, R. Hussain, G. Siligardi and L. Calzolai, Measuring protein structure and stability of protein-nanoparticle systems with synchrotron radiation circular dichroism, *Nano Lett.*, 2011, **11**, 4480–4484.

31 L. M. Gordon, K. Y. Lee, M. M. Lipp, J. A. Zasadzinski, F. J. Walther, M. A. Sherman and A. J. Waring, Conformational mapping of the N-terminal segment of surfactant protein B in lipid using 13C-enhanced Fourier transform infrared spectroscopy, *J. Pept. Res.*, 2000, **55**, 330–347.

32 R. R. Sinden, in *DNA Structure and Function*, ed. R. R. Sinden, Academic Press, San Diego, 1994, pp. 287–325, DOI: 10.1016/B978-0-08-057173-7.50013-4.

33 D. Docter, D. Westmeier, M. Markiewicz, S. Stolte, S. K. Knauer and R. H. Stauber, The nanoparticle biomolecule corona: lessons learned – challenge accepted?, *Chem. Soc. Rev.*, 2015, **44**, 6094–6121.

34 C. A. Schneider, W. S. Rasband and K. W. Eliceiri, NIH Image to ImageJ: 25 years of image analysis, *Nat. Methods*, 2012, **9**, 671–675.

35 R. Hussain, T. Jávorfi, T. R. Rudd and G. Siligardi, High-throughput SRCD using multi-well plates and its applications, *Sci. Rep.*, 2016, **6**, 38028.

36 R. Hussain, T. Jávorfi and G. Siligardi, Circular dichroism beamline B23 at the Diamond Light Source, *J. Synchrotron Radiat.*, 2012, **19**, 132–135.

37 R. Hussain, T. Jávorfi and G. Siligardi, in *Comprehensive Chirality*, ed. E. M. Carreira and H. Yamamoto, Elsevier, Amsterdam, 2012, pp. 438–448, DOI: 10.1016/B978-0-08-095167-6.00841-7.

38 R. Hussain and G. Siligardi, Characterisation of Conformational and Ligand Binding Properties of Membrane Proteins Using Synchrotron Radiation Circular Dichroism (SRCD), *Adv. Exp. Med. Biol.*, 2016, **922**, 43–59.

39 T. Jávorfi, R. Hussain, D. Myatt and G. Siligardi, Measuring circular dichroism in a capillary cell using the b23 synchrotron radiation CD beamline at diamond light source, *Chirality*, 2010, **22**(1E), E149–E153.

40 G. Siligardi and R. Hussain, CD spectroscopy: an essential tool for quality control of protein folding, *Methods Mol. Biol.*, 2015, **1261**, 255–276.

41 F. Zinna, C. Resta, M. Górecki, G. Pescitelli, L. Di Bari, T. Jávorfi, R. Hussain and G. Siligardi, Circular Dichroism Imaging: Mapping the Local Supramolecular Order in Thin Films of Chiral Functional Polymers, *Macromolecules*, 2017, **50**, 2054–2060.

42 R. Hussain, K. Benning, T. Javorfi, E. Longo, T. R. Rudd, B. Pulford and G. Siligardi, CDApps: integrated software for experimental planning and data processing at beamline B23, Diamond Light Source, *J. Synchrotron Radiat.*, 2015, **22**, 465–468.

43 S. W. Provencher and J. Glöckner, Estimation of globular protein secondary structure from circular dichroism, *Biochemistry*, 1981, **20**, 33–37.

44 N. Sreerama and R. W. Woody, Estimation of protein secondary structure from circular dichroism spectra: comparison of CONTIN, SELCON, and CDSSTR methods with an expanded reference set, *Anal. Biochem.*, 2000, **287**, 252–260.

45 I. H. van Stokkum, H. J. Spoelder, M. Bloemendal, R. van Grondelle and F. C. Groen, Estimation of protein secondary structure and error analysis from circular dichroism spectra, *Anal. Biochem.*, 1990, **191**, 110–118.

46 J. D. Amirkhanian and T. A. Merritt, The influence of pH on surface properties of lung surfactants, *Lung*, 1995, **173**, 243–254.

47 A. Cruz, C. Casals and J. Perez-Gil, Conformational flexibility of pulmonary surfactant proteins SP-B and SP-C, studied in aqueous organic solvents, *Biochim. Biophys. Acta*, 1995, **1255**, 68–76.

48 L. M. Gordon, S. Horvath, M. L. Longo, J. A. Zasadzinski, H. W. Taeusch, K. Faull, C. Leung and A. J. Waring, Conformation and molecular topography of the N-terminal segment of surfactant protein B in structure-promoting environments, *Protein Sci.*, 1996, **5**, 1662–1675.

49 R. S. Farver, F. D. Mills, V. C. Antharam, J. N. Chebukati, G. E. Fanucci and J. R. Long, Lipid polymorphism induced by surfactant peptide SP-B(1-25), *Biophys. J.*, 2010, **99**, 1773–1782.

50 A. Micsonai, F. Wien, É. Bulyáki, J. Kun, É. Moussong, Y. H. Lee, Y. Goto, M. Réfrégiers and J. Kardos, BeStSel: a web server for accurate protein secondary structure prediction and fold recognition from the circular dichroism spectra, *Nucleic Acids Res.*, 2018, **46**, W315–W322.

51 A. Micsonai, F. Wien, L. Kernya, Y. H. Lee, Y. Goto, M. Réfrégiers and J. Kardos, Accurate secondary structure prediction and fold recognition for circular dichroism spectroscopy, *Proc. Natl. Acad. Sci. U. S. A.*, 2015, **112**, E3095–E3103.

52 R. Capomaccio, I. O. Jimenez, P. Colpo, D. Gilliland, G. Ceccone, F. Rossi and L. Calzolai, Determination of the structure and morphology of gold nanoparticle–HSA protein complexes, *Nanoscale*, 2015, **7**, 17653–17657.

53 H. D. Hill, J. E. Millstone, M. J. Banholzer and C. A. Mirkin, The role radius of curvature plays in thiolated oligonucleotide loading on gold nanoparticles, *ACS Nano*, 2009, **3**, 418–424.

54 W. Zhang, Q. Zhang, F. Wang, L. Yuan, Z. Xu, F. Jiang and Y. Liu, Comparison of interactions between human serum albumin and silver nanoparticles of different sizes using spectroscopic methods, *Luminescence*, 2015, **30**(4), 397–404.

55 S. H. Lacerda, J. J. Park, C. Meuse, D. Pristinski, M. L. Becker, A. Karim and J. F. Douglas, Interaction of gold nanoparticles with common human blood proteins, *ACS Nano*, 2010, **4**, 365–379.

56 J. Piella, N. G. Bastús and V. Puntes, Size-Dependent Protein-Nanoparticle Interactions in Citrate-Stabilized Gold Nanoparticles: The Emergence of the Protein Corona, *Bioconjugate Chem.*, 2017, **28**, 88–97.

57 M. Lundqvist, I. Sethson and B.-H. Jonsson, Protein Adsorption onto Silica Nanoparticles: Conformational Changes Depend on the Particles' Curvature and the Protein Stability, *Langmuir*, 2004, **20**, 10639–10647.

58 P. Satzer, F. Svec, G. Sekot and A. Jungbauer, Protein adsorption onto nanoparticles induces conformational changes: Particle size dependency, kinetics, and mechanisms, *Eng. Life Sci.*, 2016, **16**, 238–246.

59 M. Mahmoudi, I. Lynch, M. R. Ejtehadi, M. P. Monopoli, F. B. Bombelli and S. Laurent, Protein–Nanoparticle Interactions: Opportunities and Challenges, *Chem. Rev.*, 2011, **111**, 5610–5637.

60 S. Qu, F. Sun, Z. Qiao, J. Li and L. Shang, In Situ Investigation on the Protein Corona Formation of Quantum Dots by Using Fluorescence Resonance Energy Transfer, *Small*, 2020, **16**, 1907633.

61 S. Khan, A. Gupta, A. Chaudhary and C. K. Nandi, Orientational switching of protein conformation as a function of nanoparticle curvature and their geometrical fitting, *J. Chem. Phys.*, 2014, **141**, 084707.

62 M. P. Monopoli, D. Walczyk, A. Campbell, G. Elia, I. Lynch, F. Baldelli Bombelli and K. A. Dawson, Physical–Chemical Aspects of Protein Corona: Relevance to in Vitro and in Vivo Biological Impacts of Nanoparticles, *J. Am. Chem. Soc.*, 2011, **133**, 2525–2534.

63 W. Lai, Q. Wang, L. Li, Z. Hu, J. Chen and Q. Fang, Interaction of gold and silver nanoparticles with human plasma: Analysis of protein corona reveals specific binding patterns, *Colloids Surf., B*, 2017, **152**, 317–325.

64 J. Pérez-Gil, A. Cruz and C. Casals, Solubility of hydrophobic surfactant proteins in organic solvent/water mixtures. Structural studies on SP-B and SP-C in aqueous organic solvents and lipids, *Biochim. Biophys. Acta*, 1993, **1168**, 261–270.

65 M. M. Lipp, K. Y. Lee, J. A. Zasadzinski and A. J. Waring, Phase and morphology changes in lipid monolayers induced by SP-B protein and its amino-terminal peptide, *Science*, 1996, **273**, 1196–1199.

66 M. Gupta, J. M. Hernández-Juviel, A. J. Waring, R. Bruni and F. J. Walther, Comparison of functional efficacy of surfactant protein B analogues in lavaged rats, *Eur. Respir. J.*, 2000, **16**, 1129–1133.

67 M. Gupta, J. M. Hernandez-Juviel, A. J. Waring and F. J. Walther, Function and inhibition sensitivity of the N-terminal segment of surfactant protein B (SP-B1-25) in preterm rabbits, *Thorax*, 2001, **56**, 871–876.

68 F. J. Walther, J. M. Hernandez-Juviel, L. M. Gordon, M. A. Sherman and A. J. Waring, Dimeric surfactant protein B peptide sp-b(1-25) in neonatal and acute respiratory distress syndrome, *Exp. Lung Res.*, 2002, **28**, 623–640.

69 R. Hussain, T. Jávorfi, C. S. Hughes and G. Siligardi, in *Radiation in Bioanalysis: Spectroscopic Techniques and Theoretical Methods*, ed. A. S. Pereira, P. Tavares and P. Limao-Vieira, Springer, Switzerland, 2019, DOI: **10.1007/978-3-030-28247-9**.

70 P.-L. Latreille, M. Le Goas, S. Salimi, J. Robert, G. De Crescenzo, D. C. Boffito, V. A. Martinez, P. Hildgen and X. Banquy, Scratching the Surface of the Protein Corona: Challenging Measurements and Controversies, *ACS Nano*, 2022, **16**, 1689–1707.

71 M. Ikegami and A. H. Jobe, Surfactant protein metabolism in vivo, *Biochim. Biophys. Acta, Mol. Basis Dis.*, 1998, **1408**, 218–225.

72 M. Ikegami, T. R. Korfhagen, M. D. Bruno, J. A. Whitsett and A. H. Jobe, Surfactant metabolism in surfactant protein A-deficient mice, *Am. J. Physiol.*, 1997, **272**, L479–L485.

73 T. Ueda, M. Ikegami, M. Henry and A. H. Jobe, Clearance of surfactant protein B from rabbit lungs, *Am. J. Physiol.*, 1995, **268**, L636–L641.

74 P. Cogo, A. Baritussio, F. Rosso, A. Gucciardi, V. Moretti, T. Badon, E. Duner, L. Zimmernann and V. P. Carnielli, Surfactant-associated protein B kinetics in vivo in newborn infants by stable isotopes, *Pediatr. Res.*, 2005, **57**, 519–522.

75 E. Da Silva, U. Vogel, K. S. Hougaard, J. Pérez-Gil, Y. Y. Zuo and J. B. Sørli, An adverse outcome pathway for lung surfactant function inhibition leading to decreased lung function, *Curr. Res. Toxicol.*, 2021, **2**, 225–236.